# TURBULENT/NON-TURBULENT INTERFACES IN EQUILIBRIUM AND NON-EQUILIBRIUM TURBULENCE

**Marco Zecchetto**
Instituto Superior Técnico, Universidade de Lisboa
Av. Rovisco Pais, 1, Lisboa 1049-001, Portugal
marco.zecchetto@tecnico.ulisboa.pt

**Tomoaki Watanabe**
Department of Aerospace Engineering
Nagoya University,
464-8603 Nagoya, Japan
watanabe.tomoaki@c.nagoya-u.jp

**Kouji Nagata**
Department of Aerospace Engineering
Nagoya University,
464-8603 Nagoya, Japan
nagata@c.nagoya-u.jp

**Carlos B. da Silva**
Instituto Superior Técnico, Universidade de Lisboa
Av. Rovisco Pais, 1, Lisboa 1049-001, Portugal
carlos.silva@ist.utl.pt

## ABSTRACT

Direct numerical simulations (DNS) of turbulent fronts created by non-equilibrium (unbalanced) turbulence are used to assess the characteristics of the turbulent/non-turbulent interface (TNTI) that separates regions of turbulent from non-turbulent (or irrotational) flow. The effects of the unbalance can be observed in the detailed shape of the conditional enstrophy magnitude, and in the magnitude of the maximum enstrophy but do not affect its main features. In particular the mean thickness of the TNTI is equal in classical or non-equilibrium turbulence *i.e.* it scales with the Kolmogorov micro-scale as previously observed at high Reynolds numbers.

## INTRODUCTION

According to the classical Richardson-Kolmogorov energy cascade picture the rate of viscous dissipation of kinetic energy at high Reynolds numbers is imposed by the inviscid dynamics of the large scale, energy carrying eddy motions (Richardson, 1922; Kolmogorov, 1941*a*,*b*). This concept however, relies on the assumption that the rate of energy transfer from the large-scales is balanced by the rate of viscous dissipation caused by the smallest scale eddies. In this case the non-dimensional dissipation rate $C_\varepsilon$, defined by

$$C_\varepsilon = \langle \varepsilon \rangle \mathscr{L} / \mathscr{U}^3, \tag{1}$$

is constant (Davidson, 2004), where $\langle \varepsilon \rangle$ is the mean dissipation rate. However, several experimental and numerical works (Valente *et al.*, 2014; Watanabe *et al.*, 2019; Takamure *et al.*, 2019) have shown that there are important flow cases/flow regions where $C_\varepsilon$ is not constant even if the flow is at very high Reynolds number and displaying the classic $-5/3$ energy spectrum over a wide wave-number range region. Indeed a power law of $C_\varepsilon \sim Re_l^n$, with $n \approx -1$ and $Re_l$ a local Reynolds number, is often observed (Vassilicos, 2015; Goto & Vassilicos, 2016) attesting a lack of equilibrium between the large and small scales of motion e.g. Valente & Vassilicos (2012); Isaza *et al.* (2014) reported a sudden transition from $C_\varepsilon \sim Re_l^{-1}$ to

$C_\varepsilon = const$ in the near and far field regions of grid-generated turbulence.

The goal of the present work is to assess the effects of non-equilibrium turbulence in the characteristics of the so-called turbulent/non-turbulence interface layer that separates many flow fields e.g. jets, into an irrotational (or non turbulent) an a turbulent region. For this purpose several direct numerical simulations (DNS) of turbulent fronts are carried out, where the turbulent core region is in an unbalanced (non-equilibrium) state.

## NUMERICAL METHOD

Direct numerical simulations (DNS) of forced homogeneous isotropic turbulence (HIT), decaying isotropic turbulence (DEC), and shear free turbulence (SFT) are carried out employing classical pseudo-spectral methods (collocation method) for spatial discretization, and a three-step third order explicit Runge-Kutta scheme for temporal advancement; the 2/3 rule is used for full de-aliasing. Periodic boundary conditions are imposed in the *x*, *y*, and *z* directions. A uniform ($\Delta x = \Delta y = \Delta z$) grid of $1024^3$ collocation points is created for all the cases in a cubic box of $2\pi$ sides. A DNS of forced homogeneous isotropic turbulence, was carried out using the forcing scheme by Alvelius (1999) with a peak forcing concentrated in the three wavenumbers centred at $k_p = 5$, and the flow has a Reynolds number of $Re_\lambda = 230$ and resolution of $k_{max}\eta = 1.5$ once the statistically stationary is attained. From this point onward the forcing scheme is turned off creating an unbalance in turbulence dynamics. Two different condition are simulated: in one case turbulence is let to evolve freely (decaying turbulence); in the other simulation the velocity fields are convoluted by an hyperbolic tangent profile that essentially conserves the velocity of the HIT simulation, and thus its vorticity, only in a central zone of $\pi/3$ width, suppressing it in the rest of the domain (shear free turbulence). In shear free turbulence (figure 1) two sharp and highly convoluted turbulent/non-turbulent interfaces (TNTI) are generated by the remaining core turbulence. As time progresses, the initial isotropic turbulence region (where $|\omega| \neq 0$) spreads into

the irrotational region (where $|\omega| = 0$) without mean shear. For comparison, another shear free turbulent simulation is performed employing the same procedure but starting from (classical) forced homogeneous isotropic turbulence in equilibrium. In order to isolate data collected at particular locations within the TNTI layer, conditional statistics in relation to the distance from a specific position within the TNTI layer are used. Due to the highly convoluted shape of the TNTI and its intermittent position, plane-by-plane statistics will invariably contain samples corresponding both to irrotational and to turbulent flow events masking the detailed local dynamics of turbulence. Conditional statistical data is obtained with a 3 steps procedure: *i*) the outer surface of the TNTI layer - the irrotational boundary (IB) - which consists in an iso-surface of vorticity magnitude $|\omega| = \sqrt{\omega_i \omega_i}$ is detected by analysing the histogram of the turbulent flow fraction of the flow; *ii*) a local 3D normal to the IB is defined at each one of the $N_x \times N_z$ points in the upper and lower shear layers that delimit a interface envelope;*iii*) any flow quantity of interest is collected at fixed distances $y_I$, by trilinear interpolation, into a grid defined on this local 3D normal, that points into the interior of the turbulent core region, so that $y_I < 0$ and $y_I > 0$ correspond to the irrotational and turbulent regions, respectively (the IB is located at $y_I = 0$). Once the procedure is completed statistical analysis is performed on the collected data set. Furthermore, the temporal evolution of $C_\varepsilon$ is calculated in a stack of planes on the turbulent core around the central plane using equation 1. Due to the flow geometry, instead of the integral scale one uses the longitudinal integral length scale $L_{11}$ computed from the one dimensional energy spectrum $E_{11}(\kappa_1)$ and the mean streamwise fluctuating velocity $u'_1$ norm is replaced by $\mathscr{U}$. The mean dissipation is computed inside the turbulent core region using a stack of 2d planes.

## RESULTS

Figure 1 shows contours of vorticity magnitude near the turbulent/non-turbulent interface layer at the start of the simulation, when the turbulent core region has characteristics of non-equilibrium turbulence (Fig. 1 a), and later during the simulation, when the flow recovers classical turbulent statistics (Fig. 1 b). As can be seen, a larger number of convolutions is imprinted in the TNTI layer at a later stage, as expected, because the integral scale of the flow typically increases with time, typical of classical turbulence. Moreover, the shape of the TNTI seems to be sharper, even if regions of more intense vorticity seem to be placed further away from the TNTI in the unbalanced (non-classical) interface layer.

The non-dimensional dissipation $C_\varepsilon$ evolves with the time, from the typical value of $C_\varepsilon \approx 0.5$ from forced isotropic turbulence until $C_\varepsilon \approx 1.0$, typical of free decaying turbulence (Fig. 2 a). During this time the non-dimensional dissipation exhibits the power law $C_\varepsilon \sim Re_\lambda^{-1.2}$ typical of non-equilibrium turbulence. Figure 2 b) shows the temporal evolution of the turbulent kinetic energy and viscous dissipation in a simulation of isotropic turbulence right after the power input is turned off. The time lag observed initially in the evolution of the two quantities is typically observed in non-equilibrium turbulence as described in Valente *et al.* (2014).

Figures 3 show conditional mean profiles of enstrophy $\omega_i \omega_i$, in relation to the distance from the TNTI, at different instants. In figures 3 (a,b) the first instants the flow field in the turbulent core region is characteristic of equilibrium turbulence, whereas in figures 3 (c,d) the evolution starts from non-equilibrium turbulence. The conditional mean profiles of

enstrophy with no normalisation (figure 3 a,c) show the typical sharp rise bridging the regions of irrotational ($y_I < 0$) and turbulent ($y_I > 0$) flow, respectively, and the expected decay of enstrophy in the turbulent core region as the flow evolves with time.

The normalisation of the conditional enstrophy profiles using the procedure outlined in Zecchetto & da Silva (2021) is shown in figure 3 (b,d). Recall that in that paper it has been shown that the shape of the conditional enstrophy, when normalised with the local Kolmogorov velocity and time scales, is universal i.e. equal in all flows, provided the Reynolds number is sufficiently high. The evolution of the profiles with time is similar whether the starting instant is in equilibrium or not. In the first 3-4 instants the flow is still evolving from the SFT initial state. For the later times the profiles begin to collapse and the shape recovered in the 2 cases is essentially the same obtained in Zecchetto & da Silva (2021). Indeed, a sharp peak of 1.5 is attained at a distance of about $10\eta$ from the turbulent non-turbulent interface and the theoretical value of 1 is attained after approximately $40\eta$. This 'self-similar' state is reached faster in equilibrium turbulence, which can be ascribed to different small scales dynamics. However, the mean thickness of the TNTI is equal in classical or non-equilibrium turbulence *i.e.* it scales with the Kolmogorov micro-scale as previously observed at high Reynolds numbers.

More details will be provided during the presentation.

## REFERENCES

Alvelius, K. 1999 Random forcing of three-dimensional homogeneous turbulence. *Physics of Fluids* **11** (7), 1880–1889.

Davidson, P. A. 2004 *Turbulence, an introduction for scientists and engineers*. Oxford University Press.

Goto, Susumu & Vassilicos, J. C. 2016 Unsteady turbulence cascades. *Phys. Rev. E* **94**, 053108.

Isaza, J.C., Salazar, R. & Warhaft, Z. 2014 On grid-generated turbulence in the near and far field regions. *Journal of Fluid Mechanics* **753**, 402–426.

Kolmogorov, A. N. 1941*a* Local structure of turbulence in an incompressible fluid for very large Reynolds numbers. *Dokl. Aka. Nauk SSSR* **30**, 301–305.

Kolmogorov, A. N. 1941*b* On degeneration of isotropic turbulence in an incompressible viscous liquid. *Dokl. Akad. Nauk. SSSR* **31**, 538–541.

Richardson, L. F. 1922 *Weather prediction by numerical process*. Cambridge university press.

Takamure, K., Sakai, Y., Ito, Y., Iwano, K. & Hayase, T. 2019 Dissipation scaling in the transition region of turbulent mixing layer. *International Journal of Heat and Fluid Flow* **75**, 77–85.

Valente, P. C., Onishi, R. & da Silva, C. B. 2014 Origin of the imbalance between energy cascade and dissipation in turbulence. *Phys. Rev. E* **90**, 023003.

Valente, P. C. & Vassilicos, J. C. 2012 Universal dissipation scaling for nonequilibrium turbulence. *Phys. Rev. Lett.* **108**, 214503.

Vassilicos, J. C. 2015 Dissipation in turbulent flows. *Annual Review of Fluid Mechanics* **47** (1), 95–114.

Watanabe, T., da Silva, C. B. & Nagata, K. 2019 Non-dimensional energy dissipation rate near the turbulent/non-turbulent interfacial layer in free shear flows and shear free turbulence. *Journal of Fluid Mechanics* **875**, 321–344.

Zecchetto, M. & da Silva, C. B. 2021 Universality of small-

scale motions within the turbulent/non-turbulent interface
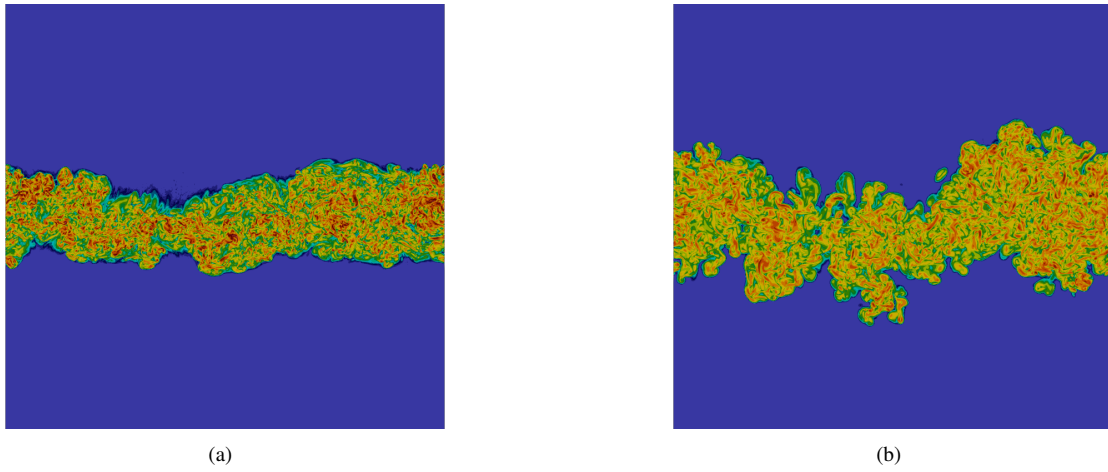layer. *Journal of Fluid Mechanics* **916**.

Figure 1.   Contours of vorticity magnitude for the shear free turbulence simulations for two instants corresponding to non-equilibrium turbulence (a) $t = 3.08$ and equilibrium turbulence (b) $t = 3.80$.
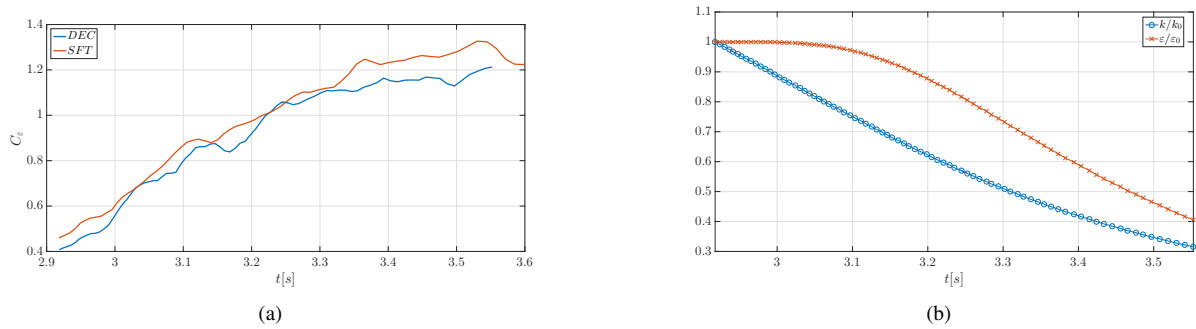


Figure 2.   (a) Evolution of the non-dimensional dissipation rate $C_\varepsilon$ with time in decaying isotropic turbulence and in shear free turbulence (computed near the centerline of the flow region); (b) Time evolution of turbulent kinetic energy and dissipation in decaying isotropic turbulence, once the forcing is turned off. The time lag observed initially in the evolution of the two quantities is typically observed in non-equilibrium turbulence.
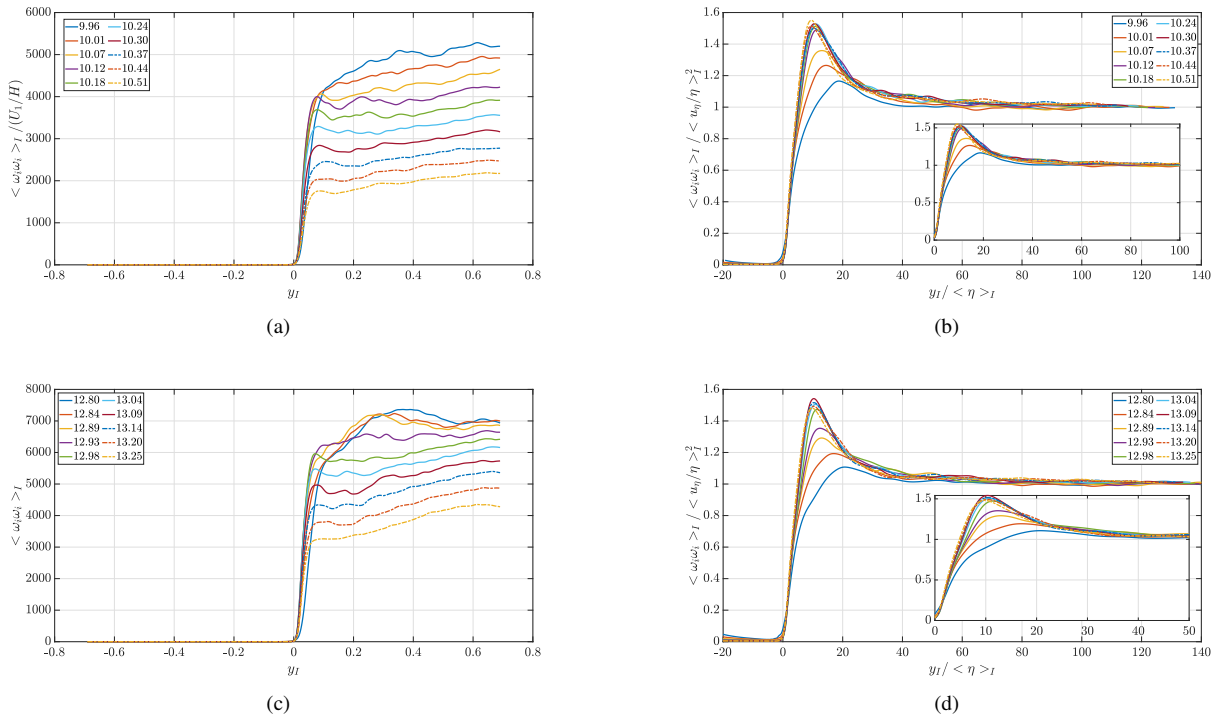
Figure 3.  Conditional mean profiles of enstrophy $\omega_i \omega_i$, in relation to the distance from the TNTI, at different instants (a,c) without normalization and (b,d) normalised by the local Kolmogorov scale. The irrotational boundary is placed at $y_I = 0$ while the non-turbulent (irrotational) and turbulent flow regions are at $y_I < 0$ and $y_I > 0$, respectively. The top figures refer to SFT starting from turbulence in equilibrium state whereas the bottom to SFT starting from non-equilibrium turbulence.